

Chemical Rate Laws and Rate Constants

RAYMOND KAPRAL, STYLIANI CONSTA AND LIAM MCWHIRTER

*Chemical Physics Theory Group, Department of Chemistry
University of Toronto, Toronto M5S 1A1, Canada*

1. – Introduction

Chemical reactions are described by mass action kinetic equations that specify how the mean concentrations of chemical species vary with time. Under what circumstances is such a description possible? How may one compute the values of the rate constants that enter these equations from a knowledge of the microscopic properties of the system?

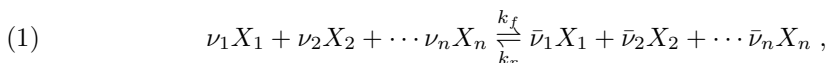
Complete answers to these questions cannot be given. However, for systems close to equilibrium where linearized versions of mass action laws apply, one may derive generalized forms of the rate laws from the microscopic evolution equations. The investigation of the conditions under which these generalized laws reduce to mass action kinetics supplies the answer to the first question.

In the course of this derivation one obtains autocorrelation function expressions for the chemical rate constants that relate these transport coefficients to the microscopic dynamics. These expressions, while exact, are formidable to compute for a many-body quantum system. Nevertheless, these correlation expressions form the starting point for a discussion of various approximate schemes for the computation of rate constants.

The derivation of the generalized chemical rate law and a discussion of the conditions under which reduction to the phenomenological form is possible are presented in Sec. 2 for a general quantum mechanical system. A detailed discussion of the properties of the rate kernel that enters this description is also presented in this section. Section 3 specializes these results to classical systems and the results are illustrated with a model of diffusive barrier crossing and a molecular dynamics study of ion solvation dynamics in water clusters. The next two sections deal with mixed quantum-classical systems. Section 4 considers the simpler case of adiabatic dynamics. Following a discussion of the reduction of the full quantum dynamics to the adiabatic mixed quantum-classical limit, a description of proton transfer in a cluster composed of polar solvent molecules is given as an example of an application. The last section considers nonadiabatic dynamics in the mixed quantum-classical limit. A discussion of some of the approximations that lead to surface hopping methods are presented and the cluster proton transfer problem is revisited to show the effects of nonadiabaticity on this reaction.

2. – Derivation of Chemical Rate Laws

2.1. Phenomenological description. – Consider a reaction among n chemical species X_i , $i = 1, \dots, n$ of the form



characterized by the forward and reverse rate constants k_f and k_r . The stoichiometric coefficients are ν_i and $\bar{\nu}_i$ for reactants and products, respectively. The mass action rate law for the average numbers \bar{N}_i of the chemical species is

$$(2) \quad \frac{d\bar{N}_i(t)}{dt} = (\nu_i - \bar{\nu}_i) \left[-k_f \prod_{j=1}^n \bar{N}_j^{\nu_j}(t) + k_r \prod_{j=1}^n \bar{N}_j^{\bar{\nu}_j}(t) \right] = (\nu_i - \bar{\nu}_i) J ,$$

The second equality defines the reaction rate J which is independent of the species label in view of the constraints on the particle number changes implied by Eq. (1).

For a reacting system at constant temperature T and volume V , the entropy change as a result of reactions is

$$(3) \quad T \frac{ds}{dt} = - \sum_{i=1}^n \mu_i \frac{d\bar{N}_i}{dt} = J \mathcal{A} ,$$

where the chemical affinity,

$$(4) \quad \mathcal{A} = \sum_{i=1}^n \mu_i (\nu_i - \bar{\nu}_i) ,$$

is the thermodynamic driving force of the chemical reaction, which vanishes at equilibrium.

Equation (2) can be used to define the progress variable $\bar{\chi}(t)$ which characterizes the extent of reaction [1]:

$$(5) \quad \frac{d\bar{\chi}(t)}{dt} = (\nu_i - \bar{\nu}_i)^{-1} \frac{d\bar{N}_i(t)}{dt} = J .$$

This equation may be integrated from time t to $t = \infty$, where the system is in equilibrium and $\bar{\chi}(\infty) = 0$, to obtain

$$(6) \quad \bar{\chi}(t) = (\nu_i - \bar{\nu}_i)^{-1} (\bar{N}_i(t) - \bar{N}_i^{eq}) .$$

Only a single dynamical variable $\bar{\chi}$ is needed to characterize the extent of reaction.

We shall be concerned with reactive systems that are perturbed slightly from chemical equilibrium so that the chemical affinity is small. We also assume that the reactive species are dilute in some chemically inert solvent so that the chemical potentials take the simple form $\mu_i = \mu_i^0 + kT \ln \bar{N}_i$. ⁽¹⁾ Expanding the average particle numbers in terms of the progress variable and linearizing in $\bar{\chi}$, we obtain

$$(7) \quad \frac{d\bar{\chi}(t)}{dt} = -k\bar{\chi}(t) ,$$

⁽¹⁾ For nonideal systems the chemical potential is expressed in terms of the activity. One may also question whether the phenomenological rate law, Eq. (2), should also be written in terms of activities. For a discussion of this issue see Ref. [2].

where the rate constant k is given by

$$(8) \quad k = \sum_{j=1}^n (\nu_j - \bar{\nu}_j) \left[k_f \prod_{i=1}^n (\bar{N}_i^{eq})^{\nu_i} \frac{\nu_j}{\bar{N}_j^{eq}} - k_r \prod_{i=1}^n (\bar{N}_i^{eq})^{\bar{\nu}_i} \frac{\bar{\nu}_j}{\bar{N}_j^{eq}} \right] .$$

From this expression we see that the rate constant k depends on both the forward and reverse rate constants and, in general, on the equilibrium concentrations. In the simple case of a linear interconversion reaction of the form



which shall primarily concern us here, k takes the simple form $k = k_f + k_r$. Finally, we note that Eq. (7) may be integrated to yield

$$(10) \quad \bar{\chi}(t) - \bar{\chi}(0) = -k \int_0^t dt' \bar{\chi}(t - t') ,$$

which will prove to be a useful form in the discussion that follows.

2.2. Nonequilibrium initial ensemble. – From Eqs. (3) and (5) we observe that the affinity \mathcal{A} , the thermodynamic driving force, is conjugate to the flux of the progress variable $\dot{\bar{\chi}}$. In order to appreciate some of the ingredients necessary to construct a microscopic description of the reactive process we consider an initial nonequilibrium ensemble where only the progress variable is constrained to deviate from its zero equilibrium value. We consider a quantum mechanical system and suppose that the microscopic Hermitian operator corresponding to the progress variable is $\hat{\chi}$. (Henceforth, a hat on a symbol will denote a quantum mechanical operator.) We shall discuss specific forms for $\hat{\chi}$ later. ⁽²⁾

The nonequilibrium ensemble for the system at constant temperature T and volume V may be constructed from the usual canonical distribution by appending an additional term $\hat{\chi}\mathcal{A}$ to the Hamiltonian \hat{H} of the system:

$$(11) \quad \hat{\rho}(0) = \frac{e^{-\beta(\hat{H} - \hat{\chi}\mathcal{A})}}{\text{Tr}e^{-\beta(\hat{H} - \hat{\chi}\mathcal{A})}} ,$$

where $\beta = (kT)^{-1}$ as usual. It then follows that the average value of the progress variable is given by

$$(12) \quad \bar{\chi}(t) = \text{Tr}\hat{\chi}(t)\hat{\rho}(0) .$$

Using the operator identity

$$(13) \quad e^{-\beta(\hat{H} - \hat{\chi}\mathcal{A})} = e^{-\beta\hat{H}} + \int_0^\beta d\lambda e^{-\lambda\hat{H}} \hat{\chi}\mathcal{A} e^{-(\beta-\lambda)\hat{H}} ,$$

we may write the linearized form of $\hat{\rho}(0)$ as

$$(14) \quad \hat{\rho}(0) = \hat{\rho}_e + \int_0^\beta d\lambda e^{-\lambda\hat{H}} \hat{\chi} e^{\lambda\hat{H}} \hat{\rho}_e \mathcal{A} ,$$

⁽²⁾ A formal discussion of species operators may be found in Ref. [3]

from which it follows that

$$(15) \quad \bar{\chi}(t) = \text{Tr} \int_0^\beta d\lambda \hat{\chi}(t) e^{-\lambda \hat{H}} \hat{\chi} e^{\lambda \hat{H}} \hat{\rho}_e \mathcal{A} = (\hat{\chi}(t), \hat{\chi}) \beta \mathcal{A} .$$

Here $\hat{\rho}_e$ is the equilibrium density matrix,

$$(16) \quad \hat{\rho}_e = \frac{e^{-\beta \hat{H}}}{\text{Tr} e^{-\beta \hat{H}}} ,$$

and the Kubo transformed correlation function is defined as [4]

$$(17) \quad (\hat{A}, \hat{B}^\dagger) = \beta^{-1} \int_0^\beta d\lambda \hat{A} e^{-\lambda \hat{H}} \hat{B}^\dagger e^{\lambda \hat{H}} \hat{\rho}_e .$$

From Eq. (15) one observes that near equilibrium the nonequilibrium average of $\hat{\chi}(t)$ is given by the autocorrelation function describing the fluctuations of the progress variable about equilibrium.

2.3. Rate law derivation. – To derive the chemical rate law [5] one starts from the Heisenberg equation of motion for $\hat{\chi}$,

$$(18) \quad \frac{d\hat{\chi}(t)}{dt} = \frac{i}{\hbar} [\hat{H}, \hat{\chi}(t)] = i \hat{\mathcal{L}} \hat{\chi}(t) = e^{i \hat{\mathcal{L}} t} i \hat{\mathcal{L}} \hat{\chi} ,$$

and extracts the evolution proportional to $\hat{\chi}(t)$ using projection operator methods. [6, 7] In view of the above considerations an appropriate projection operator is

$$(19) \quad \hat{\mathcal{P}} \hat{\mathcal{O}} = (\hat{\mathcal{O}}, \hat{\chi})(\hat{\chi}, \hat{\chi})^{-1} \hat{\chi} ,$$

since $\hat{\mathcal{P}}$ just projects $\hat{\mathcal{O}}$ onto $\hat{\chi}$. Substituting the operator identity

$$(20) \quad e^{i \hat{\mathcal{L}} t} = \int_0^t d\tau e^{i \hat{\mathcal{L}}(t-\tau)} \hat{\mathcal{P}} i \hat{\mathcal{L}} e^{i \hat{\mathcal{Q}} \hat{\mathcal{L}} \tau} + e^{i \hat{\mathcal{Q}} \hat{\mathcal{L}} t} ,$$

where $\hat{\mathcal{Q}} = 1 - \hat{\mathcal{P}}$, into the last equality in Eq. (18) we obtain the generalized Langevin equation for $\hat{\chi}(t)$:

$$(21) \quad \frac{d\hat{\chi}(t)}{dt} = - \int_0^t d\tau \tilde{k}(\tau) \hat{\chi}(t-\tau) + \hat{R}(t) ,$$

where the rate kernel is defined as

$$(22) \quad \tilde{k}(\tau) = (e^{i \hat{\mathcal{Q}} \hat{\mathcal{L}} \tau} i \hat{\mathcal{L}} \hat{\chi}, i \hat{\mathcal{L}} \hat{\chi})(\hat{\chi}, \hat{\chi})^{-1} .$$

The random reactive flux $\hat{R}(t)$ is

$$(23) \quad \hat{R}(t) = e^{i \hat{\mathcal{Q}} \hat{\mathcal{L}} t} i \hat{\mathcal{L}} \hat{\chi} .$$

Since $\text{Tr} \hat{\rho}(0) \hat{R}(t) = 0$, the average of Eq. (21) over the initial nonequilibrium ensemble yields the generalized chemical rate law,

$$(24) \quad \frac{d\bar{\chi}(t)}{dt} = - \int_0^t d\tau \tilde{k}(\tau) \bar{\chi}(t-\tau) .$$

Using Eq. (15), we also note that this equation can be written as

$$(25) \quad \frac{dC_\chi(t)}{dt} = - \int_0^t d\tau \tilde{k}(\tau) C_\chi(t - \tau) ,$$

where $C_\chi(t) = (\hat{\chi}(t), \hat{\chi})(\hat{\chi}, \hat{\chi})^{-1}$ is the normalized progress variable autocorrelation function. This equation establishes the fact that we may monitor either the decay of the progress variable fluctuations about equilibrium or the decay of nonequilibrium initial states to determine the rate constant.

It is convenient to integrate Eq. (24) over time in order to express the time evolution of the progress variable as

$$(26) \quad \bar{\chi}(t) - \bar{\chi}(0) = - \int_0^t dt' \tilde{K}(t') \bar{\chi}(t - t') ,$$

which involves the new rate kernel

$$(27) \quad \tilde{K}(t) = \int_0^t d\tau \tilde{k}(\tau) = (e^{i\hat{Q}\hat{\mathcal{L}}t} \hat{\chi}, i\hat{\mathcal{L}}\hat{\chi})(\hat{\chi}, \hat{\chi})^{-1} .$$

This kernel may also be written as

$$(28) \quad \tilde{K}(t) = \frac{1}{-i\hbar\beta} \text{Tr}[\hat{\chi}, e^{i\hat{Q}\hat{\mathcal{L}}t} \hat{\chi}] \hat{\rho}_e(\hat{\chi}, \hat{\chi})^{-1} .$$

We next consider the conditions under which the generalized rate laws, Eqs. (24) or (26), reduce to their phenomenological forms, Eqs. (7) or (10), respectively. In order to do this we need to examine the structure of the rate kernels.

2.4. Structure of the rate kernel. – Since $[\hat{\chi}, \hat{\chi}] = 0$, we see from Eq. (28) that the initial value of the rate kernel is zero, $\tilde{K}(0) = 0$. The projection operator $\hat{\mathcal{P}}$ was constructed to project out of the dynamics of any operator that part which is proportional to the progress variable $\hat{\chi}$. Consequently, since the reactive flux autocorrelation function $\tilde{k}(t)$ evolves by projected dynamics $i\hat{Q}\hat{\mathcal{L}}$, it will decay to zero on a microscopic time scale provided there are no other slowly varying degrees of freedom in the system other than $\hat{\chi}(t)$.⁽³⁾ In this circumstance $\bar{\chi}(t)$ will decay much more slowly than $\tilde{k}(t)$ and we may take $\hat{\chi}(t)$ out of the integral in Eq. (24) for times $t \gg t_{mic}$, the microscopic decay time of $\tilde{k}(t)$. If t^* is a time such that $t_{mic} \ll t^* \ll t_{chem}$ we may write

$$(29) \quad \frac{d\bar{\chi}(t)}{dt} \simeq - \left[\int_0^{t^*} d\tau \tilde{k}(\tau) \right] \bar{\chi}(t) .$$

By time t^* , $\tilde{k}(t)$ will have decayed essentially to zero and we may extend the integral to infinity and identify the rate constant k by the infinite time integral of the reactive flux autocorrelation function,

$$(30) \quad k = \int_0^\infty dt \tilde{k}(t) ,$$

⁽³⁾ If the species densities (progress variable) are slow variables, nonlinear products of local species density fields will also be slow variables. If such nonlinear variables are explicitly included in the definition of the projection operator one may explicitly separate out diffusion contributions to the rate constant. [8] These contributions will be dominant in some circumstances, for large particles for example, and allow one to microscopically derive the interplay between kinetic and diffusion-influenced rate contributions. [9]

in analogy with autocorrelation function expressions for other thermal transport coefficient expressions. Similarly, on the basis of these considerations, we see that the generalized rate law, Eq. (26), will reduce to the phenomenological form, Eq. (10), for times longer than t_{mic} where $\tilde{K}(t)$ assumes its asymptotic value k and may be removed from under the integral:

$$\begin{aligned} \bar{\chi}(t) - \bar{\chi}(0) &= - \int_0^t dt' \tilde{K}(t') \bar{\chi}(t-t'), \\ (31) \quad &\rightarrow -k \int_0^t dt' \bar{\chi}(t-t'), \quad (t \gg t_{mic}). \end{aligned}$$

So we have $\tilde{K}(\infty) = k$.

Next, we consider the consequences of replacing projected dynamics by ordinary dynamics

$$(32) \quad e^{i\hat{Q}\hat{\mathcal{L}}t}\hat{\chi} \rightarrow e^{i\hat{\mathcal{L}}t}\hat{\chi} \equiv \hat{\chi}(t),$$

in the rate kernel expressions so that the rate kernel $\tilde{K}(t)$ takes the form

$$(33) \quad K(t) = (\hat{\chi}(t), i\hat{\mathcal{L}}\hat{\chi})(\hat{\chi}, \hat{\chi})^{-1} = \frac{1}{-i\hbar\beta} \text{Tr}[\hat{\chi}, \hat{\chi}(t)] \hat{\rho}_e(\hat{\chi}, \hat{\chi})^{-1},$$

while $\tilde{k}(t)$ becomes

$$(34) \quad k(t) = (i\hat{\mathcal{L}}\hat{\chi}(t), i\hat{\mathcal{L}}\hat{\chi})(\hat{\chi}, \hat{\chi})^{-1}.$$

The tilde will be dropped when the operators or variables evolve by ordinary dynamics.

It is not difficult to establish a relation between the reactive flux rate kernels $\tilde{k}(t)$ and $k(t)$ for projected and unprojected dynamics, respectively. Differentiating Eq. (25) we obtain

$$(35) \quad k(t) = -\tilde{k}(t) - \int_0^t d\tau \tilde{k}(\tau) \frac{d}{dt} C_\chi(t-\tau),$$

whose Laplace transform is

$$(36) \quad k(z) = -\tilde{k}(z) - \tilde{k}(z)[zC_\chi(z) - 1].$$

Here the Laplace transform of any function $f(t)$

$$(37) \quad f(z) = \int_0^\infty dt e^{-zt} f(t),$$

is denoted by the same symbol but with argument z . Using the fact that

$$(38) \quad C_\chi(z) = (z + \tilde{k}(z))^{-1},$$

we obtain

$$(39) \quad k(z) = \frac{z\tilde{k}(z)}{z + \tilde{k}(z)}.$$

Note that since

$$(40) \quad \lim_{z \rightarrow 0} \tilde{k}(z) = \int_0^\infty d\tau \tilde{k}(\tau) \equiv \tilde{K}(t = \infty) = k,$$

we have

$$(41) \quad \lim_{z \rightarrow 0} K(z) = K(t = \infty) = 0 :$$

the rate kernel with unprojected dynamics decays to zero rather than to the rate constant k . The long time decay of $K(t)$ may be determined from the small z behavior of Eq. (39):

$$(42) \quad \tilde{k}(z) \approx k, \quad K(z) = \frac{k(z)}{z} \approx \frac{k}{z+k},$$

from which it follows that

$$(43) \quad K(t) \approx ke^{-kt}.$$

Since $\tilde{k}(z) = zk(z)/(z - k(z))$, the large frequency behavior of both kernels is the same, $\tilde{k}(z) \approx k(z)$ (z large), so that the short time structure of both kernels is the same. Costley and Pechukas [10] showed that $C_\chi(t) \sim t^{3/2}$ for short times so $\tilde{K}(t) \sim t^{1/2}$ and $K(t) \sim t^{1/2}$ and both kernels grow parabolically. Similarly, both $\tilde{k}(t)$ and $k(t)$ diverge as $t^{-1/2}$ for short times. As a result of these considerations we may sketch the graphs of both $\tilde{K}(t)$ and $K(t)$ and these are shown in Fig. 1. Thus, provided the

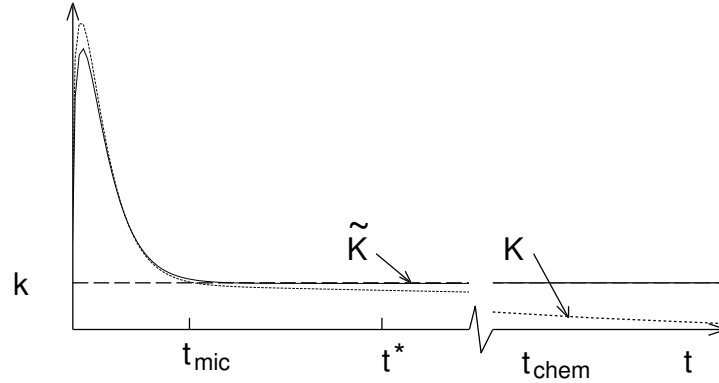


Fig. 1. – Sketch of projected $\tilde{K}(t)$ and unprojected $K(t)$ rate kernels versus time for a quantum mechanical system.

chemical relaxation time is much longer than any microscopic relaxation time in the system, $t_{chem} = k^{-1} \gg t_{mic}$, $K(t)$ will first decay on a time scale t_{mic} to a plateau value given by $K(t^*)$, $t_{mic} \ll t^* \ll t_{chem}$, followed by a slow decay to zero. [11] In this circumstance

$$(44) \quad k \approx K(t^*) = (\hat{\chi}(t^*), i\hat{\mathcal{L}}\hat{\chi})(\hat{\chi}, \hat{\chi})^{-1} = \frac{1}{-i\hbar\beta} \text{Tr}[\hat{\chi}, \hat{\chi}(t^*)]\hat{\rho}_e(\hat{\chi}, \hat{\chi})^{-1},$$

the result derived by Yamamoto [12] from linear response theory. Should such time scale separation not obtain, then the generalized rate law, Eqs. (24) or (26), must be used and the rate kernel evolution must be computed using projected dynamics.

3. – Classical Systems

If the system is classical the above derivation may be repeated with the quantum Liouville operator $i\hat{\mathcal{L}}$ replaced by its classical counterpart,

$$(45) \quad i\mathcal{L}\cdot = \{H, \cdot\},$$

where $\{\cdot, \cdot\}$ is the Poisson bracket and $H(R, P)$ is the classical Hamiltonian. The trace over the equilibrium density matrix is replaced by the classical canonical ensemble average:

$$(46) \quad \langle \dots \rangle = \frac{\int dRdPe^{-\beta H(R,P)} \dots}{\int dRdPe^{-\beta H(R,P)}} \equiv \int dRdP \rho_e(R, P) \dots .$$

The rate kernel takes the form

$$(47) \quad \tilde{K}(t) = \langle (i\mathcal{L}\chi)e^{i\mathcal{Q}\mathcal{L}t}\chi \rangle \langle \chi\chi \rangle^{-1} = \langle \{\chi, e^{i\mathcal{Q}\mathcal{L}t}\chi\} \rangle \langle \chi\chi \rangle^{-1} .$$

As in the quantum mechanical case we may consider the rate kernel $K(t)$ where projected dynamics is replaced by ordinary time evolution:

$$(48) \quad \chi(t) = e^{i\mathcal{L}t}\chi ,$$

so that

$$(49) \quad K(t) = \langle \dot{\chi}\chi(t) \rangle \langle \chi\chi \rangle^{-1} = \langle \{\chi, \chi(t)\} \rangle \langle \chi\chi \rangle^{-1} .$$

In order to examine the structure of the classical rate kernel consider a simple system with a single reactive degree of freedom q governed by a double-well free energy potential $W(q)$ shown in Fig. 2. In this case the dynamical variable corresponding to the progress

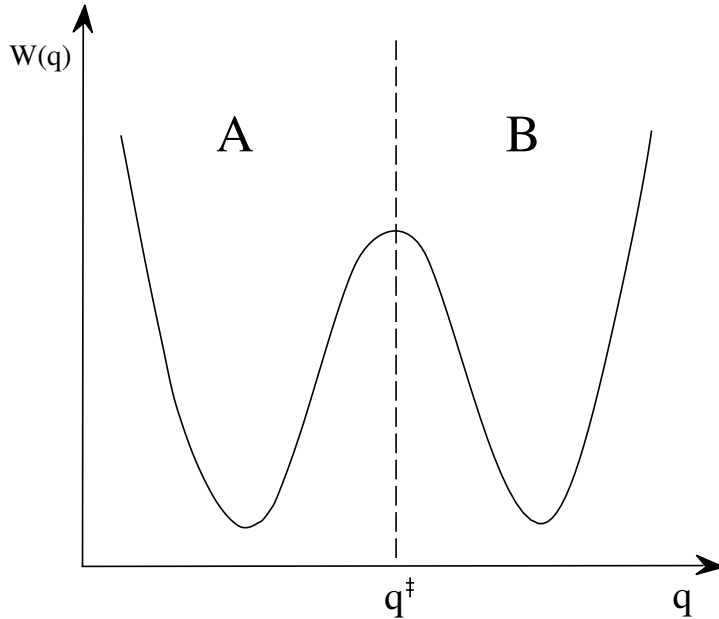


Fig. 2. – Free energy along the reaction coordinate showing the reactant and product regions separated by a free energy barrier at q^\ddagger .

variable simply monitors if the coordinate q lies to the left (species A) or to the right (species B) of the transition state at q^\ddagger :

$$(50) \quad \chi(q) = \theta(q^\ddagger - q) - \langle \theta(q^\ddagger - q) \rangle .$$

Here $\theta(q)$ is the Heaviside function. The rate kernel may be written more explicitly as

$$(51) \quad K(t) = \langle \dot{q} \delta(q - q^\ddagger) \theta(q(t) - q^\ddagger) \rangle \langle \chi \chi \rangle^{-1} .$$

This form for the classical rate kernel was also derived by Yamamoto. [12] The $t = 0^+$ limit of $K(t)$ yields the transition state theory expression for the rate constant. [13] For short times $t = \epsilon$, ($\epsilon > 0$), one has $q(t) \approx q^\ddagger + \epsilon \dot{q} + \mathcal{O}(\epsilon^2)$ and

$$(52) \quad \lim_{\epsilon \rightarrow 0} K(\epsilon) = \langle \dot{q} \delta(q - q^\ddagger) \theta(\dot{q}) \rangle \langle \chi \chi \rangle^{-1} = \langle \dot{q} \theta(\dot{q}) \rangle \langle \delta(q - q^\ddagger) \rangle \langle \chi \chi \rangle^{-1} \equiv k^{\text{TST}} .$$

We may identify this quantity with the transition state theory expression for the rate constant since

$$(53) \quad \langle \delta(q - q^\ddagger) \rangle = P_u e^{-\beta W(q^\ddagger)} ,$$

where P_u is the uniform density; thus, we have

$$(54) \quad k^{\text{TST}} = \frac{\langle |\dot{q}| \rangle}{\langle \chi \chi \rangle} P_u e^{-\beta W(q^\ddagger)} .$$

In contrast to the quantum case where the $t = 0$ value of the rate kernel is zero, the classical expression has a finite value at $t = 0^+$ and the rate kernel takes the form sketched in Fig. 3.

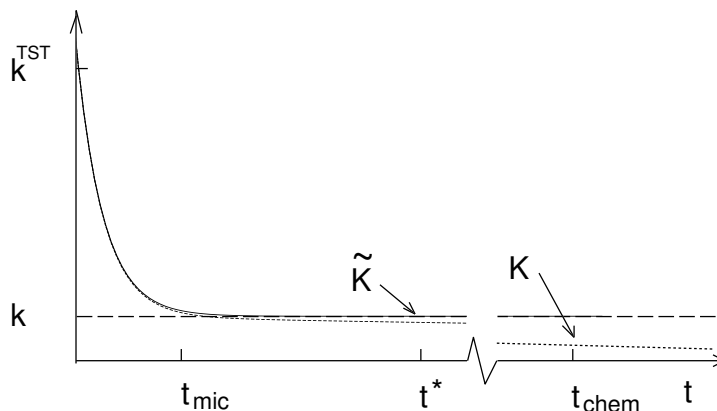


Fig. 3. – Sketch of projected $\tilde{K}(t)$ and unprojected $K(t)$ rate kernels versus time for a classical system.

The above results may be generalized to any many-body reaction coordinate $\xi(R)$. In this case the progress variable is defined analogously to Eq. (50),

$$(55) \quad \chi(\xi(R)) = \theta(\xi^\ddagger - \xi(R)) - \langle \theta(\xi^\ddagger - \xi(R)) \rangle .$$

where the generalized reaction coordinate $\xi(R)$ takes the place of q . The formal expressions for the rate kernel are similar to those derived above:

$$(56) \quad K(t) = \langle \dot{\xi} \delta(\xi - \xi^\ddagger) \theta(\xi(t) - \xi^\ddagger) \rangle \langle \chi \chi \rangle^{-1} ;$$

however, the transition state result does not always assume a simple form since it may not be possible to factor the coordinate and velocity parts of this expression as was done in Eq. (54). Examples of such complex reaction coordinates will be considered below. Equation (56) forms the basis for a computational algorithm for evaluating the rate constant for rare reactive events. [13] The rate kernel may be written as the product of the transition state rate constant, k^{TST} , and a time dependent transmission coefficient, $\kappa(t)$,⁽⁴⁾

$$(57) \quad K(t) \equiv k^{\text{TST}} \kappa(t) .$$

Once the coordinate $\xi(R)$ has been selected, the first step in the calculation is the determination of the free energy along the generalized reaction coordinate. The free energy may be computed using constrained molecular dynamics [14] or umbrella sampling [15]. The minima in the free energy may be identified with the stable chemical species and the maxima (saddle points) with the transition states separating these species. The transition state rate constant is given by the $t = 0^+$ value of the rate kernel,

$$(58) \quad k^{\text{TST}} = \langle \dot{\xi} \theta(\dot{\xi}) \delta(\xi - \xi^\ddagger) \rangle \langle \chi \chi \rangle^{-1} .$$

The transmission coefficient can be calculated by selecting configurations with the system constrained to the barrier top, $\xi = \xi^\ddagger$, releasing the constraint and determining the recrossing correction from

$$(59) \quad \kappa(t) = \frac{\langle \dot{\xi} \delta(\xi - \xi^\ddagger) \theta(\xi(t) - \xi^\ddagger) \rangle}{\langle \dot{\xi} \theta(\dot{\xi}) \delta(\xi - \xi^\ddagger) \rangle} .$$

The implementation of this method using constrained molecular dynamics is described in Refs. [14] and [16]. If $\kappa(t)$ is observed to decay to a plateau value on a microscopic time scale, well separated from the chemical relaxation time, the rate constant k can be determined directly from this plateau. If such a plateau is not observed this signals the breakdown of the phenomenological rate description and projected dynamics must be used to describe the rate kernel evolution. In the following two subsections we shall provide examples of the consequences of such breakdown and the use of projected dynamics, as well as an application of the classical reactive flux formalism for rate constant computations.

3.1. Diffusive barrier crossing: projected versus ordinary dynamics. – In order to quantitatively examine some of the features of projected dynamics we consider again the double well free energy discussed above but assume that full molecular dynamics is replaced by a diffusion model:

$$(60) \quad \frac{\partial \rho(q, t)}{\partial t} = - \frac{\partial}{\partial q} [F(q) \rho(q, t)] + D \frac{\partial^2}{\partial q^2} \rho(q, t) \equiv \mathcal{L}_{FP} \rho(q, t) .$$

This equation defines the Fokker-Planck operator \mathcal{L}_{FP} . Here $F(q) = -dW(q)/dq$ is the mean force. The equation of motion for the progress variable $\chi(q, t) = \chi(t)$ (or any other dynamical variable) is

$$(61) \quad \frac{d\chi(t)}{dt} = \mathcal{L}_{FP}^\dagger \chi(t) ,$$

⁽⁴⁾ While k^{TST} and $\kappa(t^*)$ individually depend on the choice of dividing surface ξ^\ddagger , the rate constant k does not, provided a rate law exists.

where the adjoint Fokker-Planck operator is

$$(62) \quad \mathcal{L}_{FP}^\dagger = F(q) \frac{\partial}{\partial q} + D \frac{\partial^2}{\partial q^2} .$$

The classical formulas derived above apply directly to this problem if the classical Liouville operator $i\mathcal{L}$ is replaced by the adjoint Fokker-Planck operator \mathcal{L}_{FP}^\dagger and the phase space equilibrium averages are replaced by configuration space averages over the stationary distribution of Eq. (60):

$$(63) \quad \langle \cdots \rangle = \int_{-\infty}^{\infty} dq \rho_e(q) \cdots ,$$

where

$$(64) \quad \rho_e(q) = \frac{e^{-W(q)/D}}{\int dq e^{-W(q)/D}} .$$

In order to compute the rate kernels $\tilde{K}(t)$ and $K(t)$ we need to consider the eigenvalue problems for the $\mathcal{Q}\mathcal{L}_{FP}$ and \mathcal{L}_{FP} operators as well as the $(\mathcal{Q}\mathcal{L}_{FP})^\dagger$ and \mathcal{L}_{FP}^\dagger adjoint operators:

$$(65) \quad \mathcal{L}_{FP}\psi_n(q) = -\lambda_n\psi_n(q) , \quad \mathcal{Q}\mathcal{L}_{FP}\phi_n(q) = -\mu_n\phi_n(q) ,$$

and

$$(66) \quad \mathcal{L}_{FP}^\dagger\psi_n^\dagger(q) = -\lambda_n\psi_n^\dagger(q) , \quad (\mathcal{Q}\mathcal{L}_{FP})^\dagger\phi_n^\dagger(q) = -\mu_n\phi_n^\dagger(q) .$$

The Fokker-Planck operator \mathcal{L}_{FP} has a zero eigenvalue and eigenfunction $\psi_0(q) = \rho_e(q)$, corresponding to total number conservation. If the $A \rightleftharpoons B$ interconversion process is activated we expect that $\lambda_1 \approx 0$ and all higher eigenvalues will be well separated from λ_1 if $\chi(q)$ is the only slow dynamical variable. In contrast, $\mathcal{Q}\mathcal{L}_{FP}$ ($(\mathcal{Q}\mathcal{L}_{FP})^\dagger$) has a doubly degenerate zero eigenvalue corresponding to total number and species conservation since the slow species variable $\chi(q)$ dynamics has been projected out of the evolution. For a symmetric double well one may establish that [17]

$$(67) \quad \mu_{2n} = \lambda_{2n} , \quad (n > 0) ,$$

and

$$(68) \quad \lambda_{2n} < \mu_{2n+1} < \lambda_{2n+1} .$$

The two eigenvalue spectra are sketched schematically in Fig. 4. We may now write the rate kernel in terms of the eigenvalues and eigenfunctions of $\mathcal{Q}\mathcal{L}_{FP}$:

$$(69) \quad \begin{aligned} \tilde{K}(t) &= \langle \chi\chi \rangle^{-1} \sum_{m=0}^{\infty} \langle \chi | \mathcal{L}_{FP} | \phi_{2m+1} \rangle \langle \phi_{2m+1} | \chi | \psi_0 \rangle e^{-\mu_{2m+1}t} , \\ &\equiv k + \sum_{m=1}^{\infty} \tilde{c}_m e^{-\mu_{2m+1}t} , \end{aligned}$$

where we have used an abstract notation: $\langle A|B \rangle = \int dq A(q)B(q)$. The even eigenstates do not contribute to the sum in view of the symmetry of the potential. For long times only

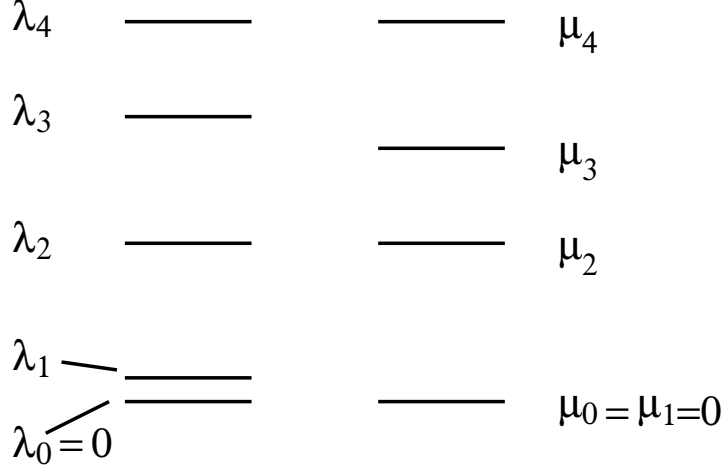


Fig. 4. – Eigenvalue spectra for the projected and unprojected Fokker-Planck operators.

the smallest non-zero eigenvalue determines the behavior. Since $\mu_1 = 0$, this eigenvalue is μ_3 and we have

$$(70) \quad \tilde{K}(t) \approx k + ce^{-\mu_3 t} .$$

We see that as expected $\tilde{K}(t)$ decays to its plateau value k on a time scale determined by μ_3 . The rate kernel has been computed for a quartic potential $W(q) = bq^4/4 - aq^2/2$, with $a = b = 1$ and diffusion coefficient $D = 50$. The decay occurs on a time scale $t_{mic} = \mu_3^{-1} \approx 0.02 \ll t_{chem} = k^{-1} \approx 0.10$. Since t_{mic} is roughly five times smaller than t_{chem} the phenomenological rate law holds approximately. For small barrier heights such time scale separation no longer holds and the rate law breaks down.

The rate constant k can be read off as the $m = 0$ coefficient in Eq. (69) and is given by

$$(71) \quad k = \langle \chi \chi \rangle^{-1} \langle \chi | \mathcal{L}_{FP} | \phi_1 \rangle \langle \phi_1 | \chi | \psi_0 \rangle = 2D\phi_1'(0) ,$$

where the second line follows from the explicit computation of the matrix elements. The eigenvector $\phi_1(q)$ may be computed analytically and is given by [17]

$$(72) \quad \phi_1(q) = \mathcal{N} e^{-W(q)/D} \int_0^q dq' e^{W(q')/D} \left[1 - 4 \int_0^{q'} dq'' \chi(q'') \rho_e(q'') \right] ,$$

where \mathcal{N} is the normalization constant:

$$(73) \quad \mathcal{N} = \left\{ 2 \int_0^\infty dq e^{-W(q)/D} \int_0^q dq' e^{W(q')/D} \left[1 - 4 \int_0^{q'} dq'' \chi(q'') \rho_e(q'') \right] \right\}^{-1} ,$$

In the limit of a high barrier, $D \ll 1$ and $a, b = \mathcal{O}(1)$, we find

$$(74) \quad k = \frac{2a}{\sqrt{2\pi}} e^{-a^2/4bD} = 4\pi\omega\omega^\ddagger e^{-\Delta W(q^\ddagger)/D} ,$$

where $\Delta W(q^\ddagger) = a^2/4b$ is the barrier height and ω and ω^\ddagger are the frequencies at the minima and barrier top, respectively. This is just Kramers' solution of the Smoluchowski equation. [18]

One may also evaluate $K(t)$ by expanding in eigenvalues and eigenfunctions of the unprojected operators:

$$(75) \quad K(t) = \langle \chi \chi \rangle^{-1} \sum_{m=0}^{\infty} \langle \chi | \mathcal{L}_{FP} | \psi_{2m+1} \rangle \langle \psi_{2m+1} | \chi | \psi_0 \rangle e^{-\lambda_{2m+1} t} .$$

Since $\lambda_1 \neq 0$ we have $\lim_{t \rightarrow \infty} K(t) = 0$ as expected. For long times we may approximate $K(t)$ by the $m = 0$ term

$$(76) \quad K(t) \approx \langle \chi \chi \rangle^{-1} \langle \chi | \mathcal{L}_{FP} | \psi_1 \rangle \langle \psi_1 | \chi | \psi_0 \rangle e^{-\lambda_1 t} .$$

In the small diffusion limit the eigenfunctions and eigenvalues of $\mathcal{Q}\mathcal{L}_{FP}$ tend to those of \mathcal{L}_{FP} so we may use ϕ_1 as an approximation for ψ_1 in a perturbation calculation of λ_1 :

$$(77) \quad \lambda_1 \approx \langle \phi_1 | \mathcal{P}\mathcal{L}_{FP} | \phi_1 \rangle = 2D\phi_1'(0) = k .$$

Thus, $K(t) \simeq ke^{-kt}$ as obtained earlier in the general case.

If colored noise models are considered, then one may also observe breakdown of the phenomenological description when the time scale of the noise process, which models the dynamics of the solvent, competes with that of the reactive event. For a discussion of such breakdown for Poisson-dichotomous-noise and BGK models see Ref. [19].

3.2. Ion solvation dynamics in clusters. – As an example of the application of the classical formalism for the calculation of reaction rates presented in this section, we consider the solvation dynamics of the ion triplet $[\text{LiCl}_2]^-$ in mesoscopic water clusters. The calculation illustrates how the free energy as a function of the ion coordinates can be used to determine the existence of chemical species, and how the rates at which these species interconvert may be calculated from the correlation function formalism developed above.

The solvation dynamics of ion pairs in bulk and cluster polar solvents has been studied and the existence of solvent-influenced ion pair species has been demonstrated. We consider a somewhat more complicated ion triplet case to show how reactions among various competing species can occur. One may compute the free energy as a function of the bond distances in the $[\text{LiCl}_2]^-$ complex to determine the possible solvation species. [20] On the basis of the results of such a calculation the reaction scheme in Fig. 5 is found to describe the solvation dynamics. There are four main species involved in the mechanism. These species will be denoted as: CIP= $[\text{Cl}|\text{Li}|\text{Cl}]^-$, the contact ion state, SSIP(1a)= $[\text{Cl}||\text{Li}|\text{Cl}]^-$ and SSIP(1b)= $[\text{Cl}|\text{Li}||\text{Cl}]^-$, ion states where Li is in intimate contact with one Cl ion and solvent-separated from the other and SSIP(2)= $[\text{Cl}||\text{Li}||\text{Cl}]^-$, the doubly solvent-separated configuration. We have not indicated dissociation channels which also exist. To fully explore this mechanism one needs to devise species operators for each of these species that partition the configuration space. Furthermore one needs to generalize the progress variable and projection operator formalism to account for the fact that more than a single progress variable is needed to characterize the mechanism.

(⁵)

(⁵) The extension of the phenomenological description to a set of progress variables may be found in Ref. [1].

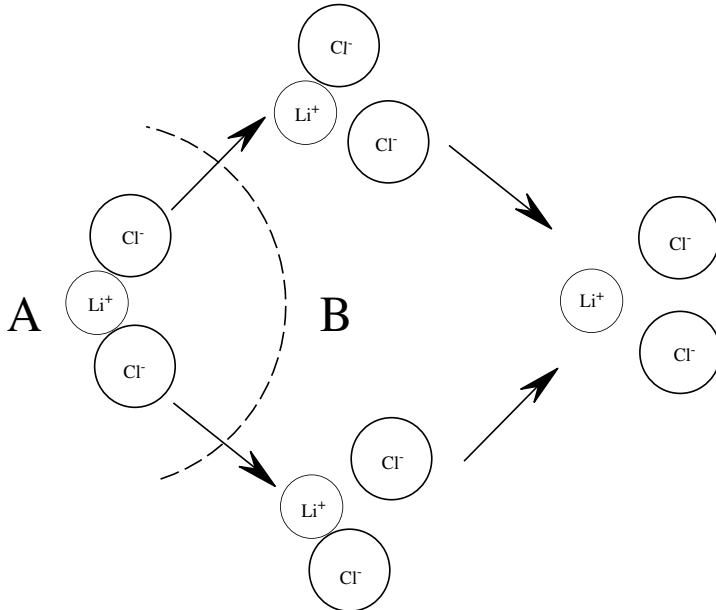


Fig. 5. – Ion solvation reaction mechanism showing transitions among the various solvation species. The dashed line separates the contact ion state A from the remainder of the species.

Rather than study this complicated situation fully, we simply focus on the CIP species, henceforth denoted by A , and group all remaining species into a single category labeled B . This reduces the problem again to an $A \rightleftharpoons B$ reaction for which the theory has been developed. In order to delineate the region of ion-complex configuration space we use as dividing line the maximum ξ^\ddagger in the free energy along the reaction coordinate

$$(78) \quad \xi(r_1, r_2) = (r_1^2 + r_2^2)^{1/2},$$

where r_1 and r_2 are the magnitudes of the distances from the Li ion to the two Cl ions, respectively. The dividing line that separates species A from “species” B is shown schematically in Fig. 5. The classical formulas, Eqs. (58) and (59), may now be used with this expression for ξ . However, from its definition one can see that even if $\xi(r_1, r_2) = \xi^\ddagger$ (or any other numerical value) the angular position in the (r_1, r_2) configuration space is not specified by this constraint. Letting the angular variable be $\phi = \arctg(r_1/r_2)$ we may plot the probability density of finding a particular value of ϕ given that the system is constrained to lie at $\xi(r_1, r_2) = \xi^\ddagger$: $P(\phi)$. This probability density, shown in Fig. 6 for a 67-molecule water cluster, has bimodal structure corresponding to the two equivalent channels leading to the SSIP(1a) and SSIP(1b) species. The minimum in $P(\phi)$ reflects the fact that direct passage from CIP to SSIP(2) is unlikely since they are separated by a free energy maximum and not a saddle.

As specified by the classical simulation algorithm, one may compute the transition state rate constant from Eq. (58), followed by a determination of the time dependent transmission coefficient from Eq. (59). For a 67-molecule, liquid-state, SPC water cluster we find $k_f^{\text{TST}} \approx 0.125 \text{ ps}^{-1}$. To estimate the transmission coefficient one needs to consider the evolution of an ensemble of statistically-independent trajectories starting from the barrier top. The configurations at the barrier top were selected every 7 ps from

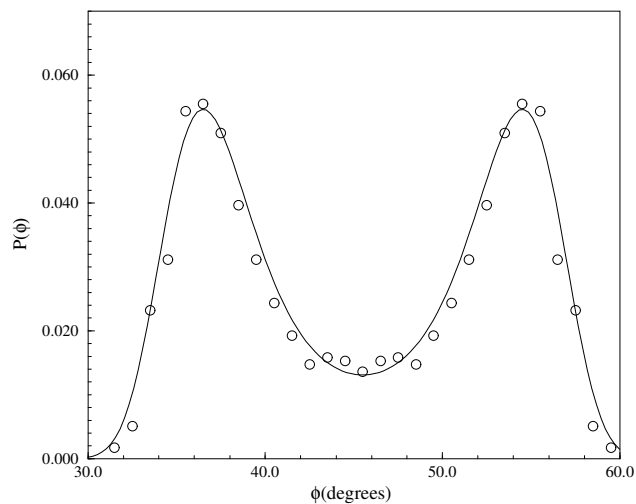


Fig. 6. – Probability density $P(\phi)$ versus ϕ for the system constrained at $\xi(r_1, r_2) = \xi^\ddagger$.

a molecular dynamics run where the reaction coordinate is constrained at the barrier top. The evolution of such an ensemble of 800 trajectories is shown in Fig. 7. On the time

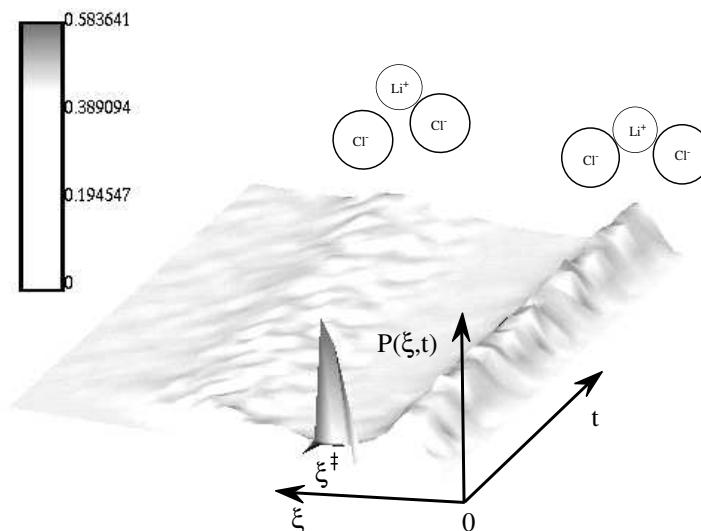


Fig. 7. – Probability distribution $P(\xi, t)$ versus ξ and t starting from the barrier top ξ^\ddagger : $P(\xi, t = 0) = \delta(\xi - \xi^\ddagger)$. The time length is 4 ps.

scale of a few tenths of a picosecond the delta-function probability splits and becomes bimodal as evolution to reactants and products occurs. From such ensembles of trajec-

tories we may compute $\kappa(t)$ and this quantity is shown in Fig. 8 for the same ensemble of trajectories as in Fig. 7. A plateau is established very quickly (≈ 0.3 ps). However,

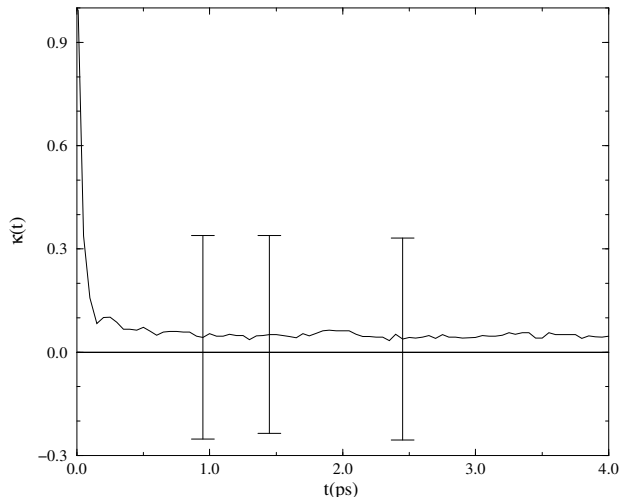


Fig. 8. – Transmission coefficient versus time for ion complex dynamics in a 67-molecule water cluster.

the plateau value is less than 0.1 indicating a significant failure of the transition state theory approximation to the rate constant. One may estimate $k_f \approx 0.005$ ps $^{-1}$.

Such small values of κ point to one of the difficulties of the straightforward application of the reactive flux correlation formalism. Large numbers of trajectories are needed to accurately estimate a small transmission coefficient and reduce the large standard deviations in the plateau region in Fig. 8. Possible schemes for improving the statistics associated with such sampling have been considered. [21, 22]

4. – Mixed Quantum-Classical Systems: Adiabatic Dynamics

For all but the simplest systems it is still not possible to carry out a full quantum mechanical calculation of the rate constants. Consequently, we shall examine systems where certain degrees of freedom are singled out for quantum mechanical treatment (quantum subsystem) while the remainder of the degrees of freedom (bath) are treated classically. We shall present results for proton transfer reactions where such a decomposition is appropriate in many circumstances. It is not a simple matter to specify the nature of such mixed quantum-classical dynamics. We shall first study adiabatic processes where the dynamics takes place on a single potential energy surface. In this limit there is no ambiguity about the form the dynamics takes. The next section will be devoted to the more general case of nonadiabatic dynamics where the situation is not so simple.

Suppose the system is described by the Hamiltonian

$$(79) \quad \hat{H} = \frac{\hat{p}^2}{2m} + \hat{V}(q) + \frac{\hat{P}^2}{2M} + \hat{V}(Q) + \hat{V}(q, Q),$$

where q and Q are the coordinates of the quantum subsystem and bath, respectively. Also, we denote the corresponding momentum operators and masses by lower and upper case letters, respectively. We shall consider the limit where the masses M of the bath particles are much larger than those of the quantum subsystem, $M \gg m$.

To begin the analysis we rewrite the trace in the quantum expression for the rate kernel $K(t)$ in Eq. (33) in the $\{Q\}$ representation for the bath degrees of freedom and retain the abstract notation for the quantum subsystem degrees of freedom:

$$(80) \quad K(t) = (\hat{\chi}, \hat{\chi})^{-1} \frac{1}{-i\hbar\beta} \text{Tr}' \int dQ \langle Q | [\hat{\chi}, \hat{\chi}(t)] \hat{\rho}_e | Q \rangle ,$$

where Tr' is a partial trace over the subsystem degrees of freedom. Next, we introduce a Wigner representation [23] of the bath degrees of freedom. The Wigner transform of any operator \hat{A} takes the form

$$(81) \quad \hat{A}_W(R, P) = \int dz e^{-iPz/\hbar} \langle R + \frac{z}{2} | \hat{A} | R - \frac{z}{2} \rangle ,$$

and the partial Wigner transform of the equilibrium density matrix is

$$(82) \quad \hat{\rho}_W(R, P) = (2\pi\hbar)^{-3N} \int dz e^{iPz/\hbar} \langle R - \frac{z}{2} | \hat{\rho}_e | R + \frac{z}{2} \rangle .$$

Note that both of these quantities are still operators in the subsystem degrees of freedom.

The evaluation of the rate kernel requires the computation of matrix elements of triple operator products whose partial Wigner representation is [24]

$$(83) \quad \int dQ \langle Q | \hat{A} \hat{B} \hat{\rho}_e | Q \rangle = \int dR dP \left(\hat{A}_W(R, P) e^{\hbar\Lambda/2i} \hat{B}_W(R, P) \right) \hat{\rho}_W(R, P) ,$$

where

$$(84) \quad \Lambda = \overleftarrow{\nabla}_P \cdot \overrightarrow{\nabla}_R - \overleftarrow{\nabla}_R \cdot \overrightarrow{\nabla}_P ,$$

and the directions of the arrows on the gradient operators indicate the directions in which these operators should be applied. Using this result the rate kernel takes the form

$$(85) \quad K(t) = (\hat{\chi}, \hat{\chi})^{-1} \frac{1}{-i\hbar\beta} \text{Tr}' \int dR dP \left(\hat{\chi}_W(R, P) e^{\hbar\Lambda/2i} \hat{\chi}_W(R, P, t) \right. \\ \left. - \hat{\chi}_W(R, P, t) e^{\hbar\Lambda/2i} \hat{\chi}_W(R, P) \right) \hat{\rho}_W(R, P) ,$$

where $\hat{\chi}_W(R, P, t) \equiv \hat{\chi}_W(t)$ is the solution of the equation of motion

$$(86) \quad \frac{d\hat{\chi}_W(t)}{dt} = \frac{i}{\hbar} \left(\hat{H}_W e^{\hbar\Lambda/2i} \hat{\chi}_W(t) - \hat{\chi}_W(t) e^{\hbar\Lambda/2i} \hat{H}_W \right) .$$

Here the partial Wigner representation of the Hamiltonian is

$$(87) \quad \hat{H}_W(R, P) = \frac{\hat{p}^2}{2m} + \hat{V}(q) + \frac{P^2}{2M} + V(R) + \hat{V}(q, R) .$$

Next, we consider the limit where the bath particles are massive compared to the those of the quantum subsystem. It is convenient to introduce scaled variables such that the

momenta of the heavy particles have the same order of magnitude as the momenta of the light particles. Consequently, we scale distances by the thermal wavelength of the light particles, $\lambda_m = (\hbar^2\beta/m)^{1/2}$, time in units of $t_0 = \beta\hbar$, and energy in units of $E_0 = \beta^{-1}$. In these scaled units the light particle momenta are scaled by $p_m = m\lambda_m/t_0 = (m/\beta)^{1/2}$ and the heavy particle momenta by $P_M = (M/\beta)^{1/2}$. In scaled units

$$(88) \quad \frac{\hbar}{2i}\Lambda \rightarrow \frac{\mu}{2i}\Lambda ,$$

and we may expand the equation of motion in the smallness parameter $\mu = (m/M)^{1/2}$. Expanding to linear order in μ and then returning to unscaled units, the equation of motion, Eq. (86), becomes

$$(89) \quad \frac{d\hat{\chi}_W(t)}{dt} = \frac{i}{\hbar}[\hat{H}_W, \hat{\chi}_W(t)] + \frac{1}{2}\left(\{\hat{\chi}_W(t), \hat{H}_W\} - \{\hat{H}_W, \hat{\chi}_W(t)\}\right) .$$

Carrying out a similar μ expansion, the rate kernel Eq. (85) takes the form:

$$(90) \quad K(t) = (\hat{\chi}, \hat{\chi})^{-1} \frac{1}{-i\hbar\beta} \text{Tr}' \int dRdP \left([\hat{\chi}_W(R, P), \hat{\chi}_W(R, P, t)] + \frac{1}{2}\left(\{\hat{\chi}_W(R, P, t), \hat{\chi}_W(R, P)\} - \{\hat{\chi}_W(R, P), \hat{\chi}_W(R, P, t)\}\right) \right) \hat{\rho}_W(R, P) .$$

As noted above these quantities still involve abstract operators in the quantum subspace. We may now work in any convenient representation and for this purpose we choose the adiabatic eigenstates of the Hamiltonian operator $\hat{h}(R) = \frac{\hat{p}^2}{2m} + \hat{V}(q) + V(R) + \hat{V}(q, R)$:

$$(91) \quad \hat{h}(R)|\alpha; R\rangle = E_\alpha(R)|\alpha; R\rangle .$$

Letting the matrix elements of an operator $\hat{A}_W(R, P)$ be denoted by $A_W^{\alpha\alpha'}(R, P)$, the equation of motion, Eq. (89), may be written in this basis as

$$(92) \quad \begin{aligned} \frac{d\chi_W^{\alpha\alpha'}(t)}{dt} &= \frac{i}{\hbar} E_{\alpha\alpha'} \chi_W^{\alpha\alpha'}(t) + \{\chi_W^{\alpha\alpha'}(t), \frac{1}{2}(H_W^\alpha + H_W^{\alpha'})\} + \\ &\quad \frac{1}{2} \sum_{\alpha''} \left((\nabla_P \chi_W^{\alpha\alpha''}(t)) \cdot \mathcal{D}_{\alpha''\alpha'} + \mathcal{D}_{\alpha\alpha''} \cdot \nabla_P \chi_W^{\alpha''\alpha'}(t) \right) - \\ &\quad \sum_{\alpha''} \frac{P}{M} \left(\chi_W^{\alpha\alpha''}(t) \cdot d_{\alpha''\alpha'} - d_{\alpha\alpha''} \cdot \chi_W^{\alpha''\alpha'}(t) \right) , \end{aligned}$$

where $H_W^\alpha(R, P) = P^2/2M + E_\alpha(R)$, $E_{\alpha\alpha'} = E_\alpha(R) - E_{\alpha'}(R)$ and $\mathcal{D}_{\alpha\alpha'} = (E_\alpha(R) - E_{\alpha'}(R))d_{\alpha\alpha'}$ with $d_{\alpha\alpha'} = \langle \alpha; R | \nabla_R | \alpha'; R \rangle$. The rate kernel may also be expressed in terms of these matrix elements to provide an in-principle method for its computation. However, Eq. (92) is quite formidable and involves coupling among all adiabatic states through the nonadiabatic coupling terms $\mathcal{D}_{\alpha\alpha'}$. The analysis presented thus far may serve as a starting point for approximate treatments of nonadiabatic dynamics for mixed quantum-classical systems.

Now we focus on the limit where the dynamics is assumed to take place on a single adiabatic surface, the adiabatic limit, and these equations take an especially simple form. The evolution equation reduces to

$$(93) \quad \frac{d\chi_W^\alpha(t)}{dt} = \{\chi_W^\alpha(t), H_W^\alpha\} ,$$

where $\chi_W^\alpha(t) = \langle \alpha; R | \hat{\chi}_W(t) | \alpha; R \rangle$. This is just a classical evolution equation but with Hellmann-Feynman forces determined by the potential $E_\alpha(R)$ obtained from the solution of the Schrödinger equation for the α adiabatic eigenstate. The rate kernel may be written in this adiabatic limit as

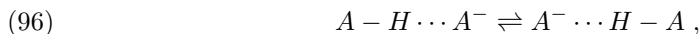
$$(94) \quad K(t) = \langle \chi^\alpha \chi^\alpha \rangle^{-1} \int dR dP \{ \chi_W^\alpha(t), \chi_W^\alpha \} \rho_W^\alpha(R, P),$$

with

$$(95) \quad \rho_W^\alpha(R, P) = \frac{e^{-\beta H_W^\alpha}}{\int dR dP e^{-\beta H_W^\alpha}}.$$

The algorithm for adiabatic mixed quantum-classical dynamics is simple. The dynamical variables depend on the classical coordinates (R, P) and the adiabatic state $|\alpha; R\rangle$. The classical coordinates evolve by Newton's equations of motion but with Hellmann-Feynman forces corresponding to the α adiabatic state. At each classical time step the Schrödinger equation is solved to determine the α adiabatic state as a function of the instantaneous position R . We shall now illustrate the application of this formalism to proton transfer in a polar molecular cluster.

4.1. *Proton transfer in molecular clusters.* – We consider proton transfer,



within a strongly hydrogen bonded proton-ion complex $[AHA]^-$ solvated by a cluster composed of model polar molecules. [25] Like the ion solvation example in the previous section, the molecular clusters we consider have tens of molecules forming one or two solvent shells around the complex. The proton transfer process is influenced by the solvent. Solvent configurations can lead to polarization effects that favor the reactant or product states in Eq. (96). The proton configuration thus attained may also polarize the solvent so that the transfer is an activated process. For strongly hydrogen bonded systems the intrinsic barrier without solvent effects is absent or negligibly small so that the solvent effects play a dominant role in determining the reaction rate. In fact, these solvent effects are responsible for the very existence of reactants and products in this reaction. Adiabatic proton transfer has been studied in bulk solvents. [26] Studies of proton transfer in molecular clusters were undertaken to determine how the finite size, presence of strong surface forces and cluster fluctuations may alter the rates and mechanisms of such reactions. We shall primarily be concerned with the illustration of the computational method but will conclude with a few remarks on what such studies have shown about cluster proton transfer mechanisms.

The first issue to address is the choice of a reaction coordinate. In view of the above discussion the solvent polarization, [27]

$$(97) \quad \xi(R) = \Delta E(R) = \sum_{i,a} z_a e \left(\frac{1}{|\mathbf{R}_i^a - \mathbf{s}|} - \frac{1}{|\mathbf{R}_i^a - \mathbf{s}'|} \right).$$

where \mathbf{s} and \mathbf{s}' are two points in the vicinities of the reactant and product configurations, is expected to reflect the differences between the reactant and product states, and we shall show that this indeed the case. In this equation the sum runs over all solvent molecules

i and atomic sites a . To confirm that the dynamics along the reaction coordinate is activated we may compute the free energy as function of $\Delta E(R)$,

$$(98) \quad W(\Delta E) \sim -kT \ln \langle \delta(\Delta E(R) - \Delta E) \rangle ,$$

where ΔE is a numerical value of $\Delta E(R)$. The free energy is displayed in Fig. 9 for a 67-molecule cluster. While the intrinsic potential for this model has a negligible barrier

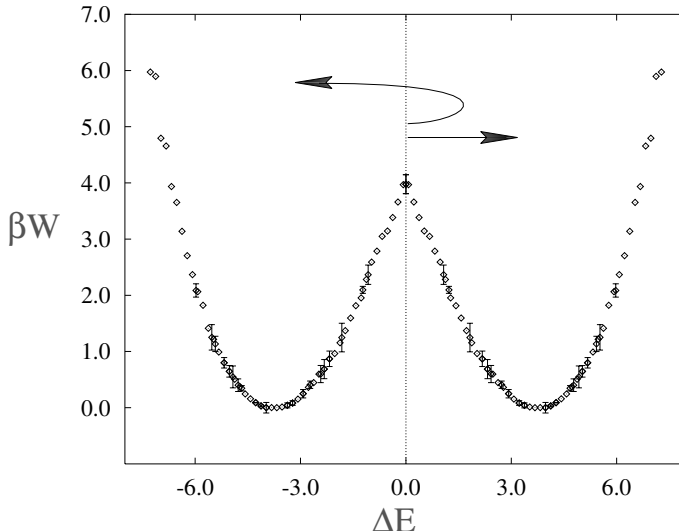


Fig. 9. – Free energy along the polarization reaction coordinate for a 67-molecule molecular cluster with molecular dipole moment $\mu = 5.0D$.

of $\approx 0.2 kT$, the free energy along ΔE has an $\approx 4.0 kT$ barrier arising from solvent polarization effects. For this symmetric reaction the transition state lies at $\Delta E = 0$. Consequently, we may define the progress variable for the reaction in terms of ΔE using the Heaviside function:

$$(99) \quad \chi(R) = \theta(\Delta E(R)) - \langle \theta(\Delta E(R)) \rangle .$$

We assume that the proton is confined to the adiabatic ground state $|0; R\rangle$ during the course of the proton transfer. At each molecular dynamics time step the protonic Schrödinger equation $\hat{h}|0; R\rangle = E_0(R)|0; R\rangle$ is solved by expanding $|0; R\rangle$ in a basis of Gaussian functions. [25] The positions and momenta of the classical bath and complex particles evolve by Newton's equations of motion:

$$(100) \quad M_i \ddot{R}_i = -\nabla_{R_i} E_0(R).$$

The temporal variation of ΔE under this adiabatic dynamics is shown in Fig. 10. The transitions between reactant and product configurations are clearly seen confirming the utility of this reaction coordinate to monitor the course of the proton transfer process.

We may now use directly the formalism developed here to compute both the transition state theory approximation to the rate constant and the time-dependent transmission

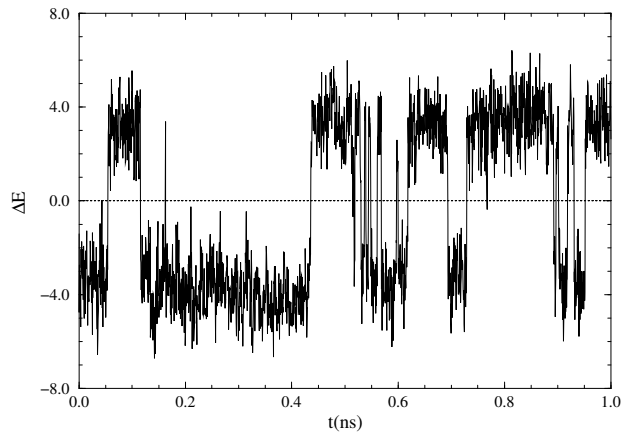


Fig. 10. – Solvent polarization (in units of $10^{-21}C/\text{\AA}$) as a function of time for a 67-molecule cluster.

coefficient. The transition state theory rate constant is given by the $t = 0^+$ value of the rate kernel,

$$(101) \quad k^{\text{TST}} = \langle \Delta \dot{E}(R) \theta(\Delta \dot{E}(R)) \delta(\Delta E(R)) \rangle \langle \chi \chi \rangle^{-1} .$$

This is an example of a many-body reaction coordinate where the position and momentum parts of the above average do not factor. Nevertheless, it is straightforward to compute the TST rate constant and we find: $k^{\text{TST}} = 0.08 \text{ ps}^{-1}$ for the 67-molecule cluster. The transmission coefficient is

$$(102) \quad \kappa(t) = \frac{\langle \Delta \dot{E}(R) \delta(\Delta E(R)) \theta(\Delta E(R(t))) \rangle}{\langle \Delta \dot{E}(R) \theta(\Delta \dot{E}(R)) \delta(\Delta E(R)) \rangle} ,$$

and it was computed using the constrained-reaction-coordinate ensemble: a holonomic constraint was applied to the equations of motion to fix $\Delta E(R) = 0$ at the transition state. Configurations were drawn at intervals from this long constrained MD trajectory and at each such point the constraint was released and the unconstrained dynamics was followed for a short time interval. The transmission coefficient could be computed using Eq. (102) when proper account of the bias introduced by the constraint was taken into account. [14] The transmission coefficient is shown in Fig. 11. It decays to a plateau value after a few picoseconds and the value of $\kappa(t^*) \approx 0.4$ can be read off this graph. The transmission coefficient accounts for recrossings of the free energy barrier top of the sort indicated schematically in Fig. 9. The full rate constant is thus $k = k^{\text{TST}} \kappa(t^*) = 0.032 \text{ ps}^{-1}$.

We close this subsection with a few remarks about the cluster proton transfer mechanism. The solvation of the complex in the cluster, dependent on the cluster size, strongly influences the mechanism. One may monitor the position of the complex relative to the center of mass in the cluster in the course of a long reactive trajectory. For the model system considered here the complex tends to reside on the surface of the cluster. For small clusters (say 20-molecule clusters with approximately one solvent shell around the

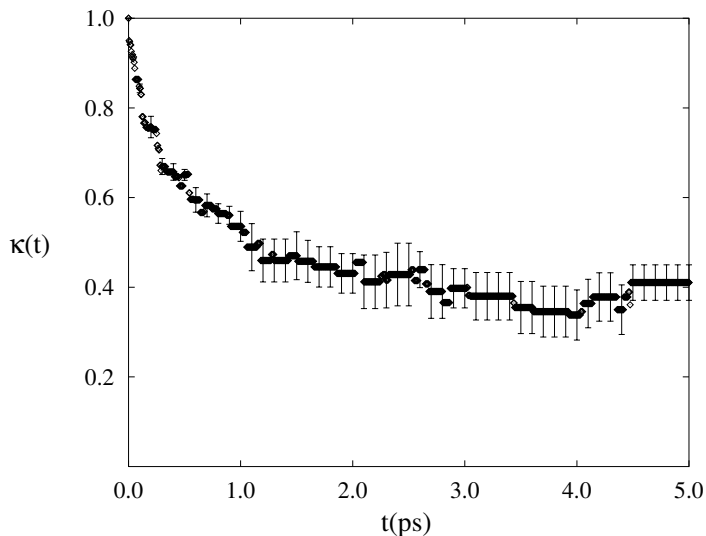


Fig. 11. – Transmission coefficient as a function of time for a 67-molecule cluster.

complex) frequent proton transfer events are correlated with excursions of the complex into the interior of the cluster. For larger clusters (say the 67-molecule cluster chosen for illustration here with approximately two solvent shells around the complex) there are again frequent proton hops when the complex penetrates at least one solvent layer into the cluster but, in addition, there are proton transfers when the complex floats on the cluster surface. In this case the proton transfer occurs by a “fishing bobbin” mechanism schematically illustrated in Fig. 12. When the proton is in the reactant configuration,

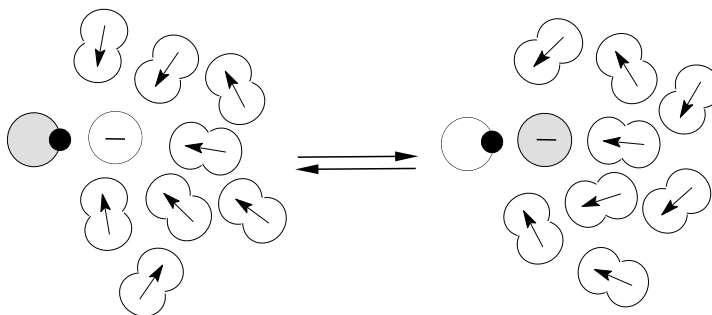


Fig. 12. – Cluster surface proton transfer mechanism. The orientation of the proton-ion complex on the surface is correlated with the position of the proton in reactant or product states within the complex.

tightly bound to the ion with solid shading, the other ion in the proton-ion complex with no shading is strongly solvated. Thus the complex attains the surface configuration shown in the figure. As a result of fluctuations the complex may assume surface configurations where it lies parallel to the surface and has a more symmetrical solvation structure. Proton transfer may occur and if it does the complex will flip its surface orientation, like a fishing bobbin on the surface of a lake, as indicated in the figure. This

is one example of some of the unusual mechanistic features one may observe in cluster reactions.

5. – Mixed Quantum-Classical Systems: Nonadiabatic Dynamics

In nonadiabatic dynamics the system is no longer restricted to evolve on a single potential energy surface and transitions among the different quantum eigenstates are possible due to the existence of the coupling terms in Eq. (92). Most molecular dynamics methods for treating the nonadiabatic case are based on surface hopping methods that represent the mixed quantum-classical dynamics by an ensemble of trajectories where the system makes hops among the various adiabatic states. [28, 29, 30, 31] While we shall not present a derivation of surface hopping methods, we shall give a discussion of some of the approximations that must be made in order to reduce the exact equations of motion to a form where a surface hopping ansatz can be made. In the second part of this section we use Tully’s surface hopping scheme [28] to treat the proton transfer dynamics without restriction to a single adiabatic potential surface.

A central element in mixed quantum-classical dynamics is the reduced propagator,

$$(103) \quad K_{\alpha_2\alpha_1}(Q_2, t''|Q_1, t') = \langle \alpha_2 Q_2 | e^{-i\hat{H}(t''-t')/\hbar} | \alpha_1 Q_1 \rangle ,$$

written in the basis $|\alpha Q\rangle = |\alpha\rangle|Q\rangle$. This propagator gives the probability amplitude for finding the quantum subsystem in the state $\alpha_2 = \langle q|\alpha_2\rangle$ and the bath with coordinates Q_2 at time t'' given that the subsystem was in the quantum state $\alpha_1 = \langle q|\alpha_1\rangle$ and the bath in Q_1 at time t' . Pechukas [32] carried out a semi-classical analysis of this propagator. In this analysis the reduced propagator is written as a path integral

$$(104) \quad K_{\alpha_2\alpha_1}(Q_2, t''|Q_1, t') = \int_{Q_1, t'}^{Q_2, t''} \mathcal{D}Q_t e^{iS_0[Q_t]/\hbar} T_{\alpha_2\alpha_1}[Q_t] ,$$

where the action is

$$(105) \quad S_0[Q_t] = \int_{t'}^{t''} dt \frac{M}{2} \dot{Q}_t^2 ,$$

and the transition amplitude is $T_{\alpha_2\alpha_1}[Q_t] = \langle \alpha_2 | \alpha_1(t''t') \rangle$ where

$$(106) \quad |\alpha_1(t''t')\rangle = \hat{T} e^{-\frac{i}{\hbar} \int_{t'}^{t''} d\tau \hat{h}(Q_\tau, q)} |\alpha_1\rangle \equiv \hat{U}(t'', t'; Q_t) |\alpha_1\rangle ,$$

is the wavefunction at time t'' found by evolution under \hat{U} with condition α_1 at time t' . The time ordering operator is \hat{T} . Pechukas assumed that the magnitude of $T_{\alpha_2\alpha_1}[Q_t]$ varies more slowly with Q_t than its phase and made a stationary phase approximation to obtain

$$(107) \quad K_{\alpha_2\alpha_1}^{QSC}(Q_2, t''|Q_1, t') = \sum_{Q_t} e^{iS_0[Q_t]/\hbar} T_{\alpha_2\alpha_1}[Q_t] N_{\alpha_2\alpha_1}[Q_t] ,$$

where $N_{\alpha_2\alpha_1}[Q_t]$ is a normalization factor and the sum runs over all “classical” paths that start at Q_1 at time t' and end at Q_2 at time t'' . (We have used the same symbol Q_t for these paths to avoid proliferation of notation.) These paths are found by solving Pechukas’ equation of motion:

$$(108) \quad M\ddot{Q}_t = -\Re\left(\langle \alpha_2(t, t'') | \frac{\partial \hat{h}_t}{\partial Q_t} | \alpha_1(t, t') \rangle / \langle \alpha_2(t, t'') | \alpha_1(t, t') \rangle\right) .$$

This equation is difficult to solve since it is nonlocal, depending on the entire history from t' to t'' , and its solutions are not unique.

We are interested in computing the the rate kernel, Eq. (80), in the mixed quantum-classical limit. Using the same basis as above, $|\alpha Q\rangle = |\alpha\rangle|Q\rangle$, we may write this kernel as,

$$(109) K(t) = \frac{-2}{\hbar\beta} \text{Tr}' \int d\mathbf{Q} \mathfrak{S} \left(\chi(Q_1) \mathbf{K}^\dagger(Q_3, t|Q_1, 0) \chi(Q_3) \mathbf{K}(Q_3, t|Q_2, 0) \right) \rho(Q_2, Q_1) .$$

We have used the notation, $\mathbf{Q} = (Q_1, Q_2, Q_3)$ and

$$(110) \quad [\chi(Q_1)]_{\alpha_1\alpha_2} = \chi_{\alpha_1\alpha_2}(Q_1) = \langle \alpha_1 Q_1 | \hat{\chi} | \alpha_2 Q_1 \rangle ,$$

while the matrix elements of the reduced propagator are

$$(111) \quad [\mathbf{K}(Q_2, t''|Q_1, t')]_{\alpha_2\alpha_1} = K_{\alpha_2\alpha_1}(Q_2, t''|Q_1, t') .$$

The equilibrium density matrix is $\rho(Q_2, Q_1)$.

Carrying out Pechukas' stationary phase analysis, the semiclassical limit $\hbar \rightarrow 0$ of the rate kernel can be evaluated to yield:

$$(112) \quad K^{QSC}(t'') = -\frac{2}{\hbar\beta} \mathfrak{S} \int d\mathbf{Q} \sum_{\gamma, \boldsymbol{\mu}, \nu} \rho_{\mu_2, \nu}(Q_2, Q_1) \chi_{\gamma_2 \mu_1}(Q_3) \chi_{\nu, \gamma_1}(Q_1) \\ \times \sum_{Q'_t} \sum_{Q_t} \exp [i(S_o[Q_t] - S_o[Q'_t])/\hbar] T_{\gamma}^*[Q'_t] T_{\boldsymbol{\mu}}[Q_t] N_{\gamma}^*[Q'_t] N_{\boldsymbol{\mu}}[Q_t] ,$$

where $\gamma = (\gamma_1, \gamma_2)$ and $\boldsymbol{\mu} = (\mu_1, \mu_2)$. Here, Q'_t and Q_t are ‘‘classical’’ paths from Q_1 to Q_3 and from Q_2 and Q_3 respectively. Evaluating this rate kernel is difficult because of a ‘‘root’’ search problem and a caustic problem. These difficulties can be avoided by switching to the initial value formalism of Miller and Heller [33, 34]; however, this switch does not eliminate the phase interference structure of the bath manifested by the factors $\exp [iS_o/\hbar] N[Q_t]$ [35]. This structure is responsible for classically forbidden dynamics or tunneling behavior for the bath degrees of freedom.

In order to make the evaluation of the rate kernel more tractable, we make a decoherence approximation which states that the dominant contributions to the rate kernel come from those paths Q'_t and Q_t which are close. ⁽⁶⁾ Given decoherence, we can replace $\int d\mathbf{Q}$ by $\int dQ_3 dQ_1 \int_{\epsilon} d\Delta Q$ where $\Delta Q = Q_1 - Q_2$. Here, ϵ is a ball centred on 0 with a small radius R_{ϵ} . Furthermore, we can replace the double sum over Q'_t and Q_t by a double restricted sum over Q'_t and Q_t , the restriction being that Q'_t and Q_t should be approximately the same. In addition to these replacements, the following approximations can be made

$$(113) \quad \exp [i(S_o[Q_t] - S_o[Q'_t])/\hbar] N_{\gamma}^*[Q'_t] N_{\boldsymbol{\mu}}[Q_t] = \\ \left(\frac{M}{2\pi\hbar} \right)^{3N} \exp \left[-iM\dot{Q}_1 \cdot \Delta Q/\hbar \right] \\ \times \left| \left(\frac{\partial Q_3(Q_1, \dot{Q}_1)}{\partial \dot{Q}_1} \right)_{\gamma} \right|^{-1/2} \left| \left(\frac{\partial Q_3(Q_1, \dot{Q}_1)}{\partial \dot{Q}_1} \right)_{\boldsymbol{\mu}} \right|^{-1/2}$$

⁽⁶⁾ The justification for such an approximation has been argued also on the basis of a stationary phase approximation of the kernel [29]

$$(114) \quad T_{\gamma}^* [Q'_t] T_{\mu} [Q_t] \approx T_{\gamma}^* [Q_t] T_{\mu} [Q_t] .$$

Two complications arise. First, for a given pair (γ, μ) no paths Q'_t and Q_t may exist which are approximately the same. Second, the Jacobi matrices $(\partial Q_t / \partial \dot{Q}_1)_{\gamma}$ and $(\partial Q_t / \partial \dot{Q}_1)_{\mu}$ satisfy two different Jacobi (Pechukas) equations: one characterized by the γ states, the other by the μ states. However, both these equations will be functionals of the same path $Q'_t = Q_t$. As a result, these matrices will not be the same. To resolve these problems, a zero back reaction approximation has been used [29] which assumes that the motion of the classical bath is insensitive to the perturbations resulting from the state changes of the quantum subsystem. Within this approximation, the two Jacobi matrices become the same and one is guaranteed to find a pair of close paths Q_t and Q'_t for any pair (γ, μ) . Therefore, the product of the Jacobian determinants in Eq. (113) becomes approximately

$$(115) \quad \left| \left(\frac{\partial Q_3(Q_1, \dot{Q}_1)}{\partial \dot{Q}_1} \right)_{\gamma} \right|^{-1}$$

Collecting together these replacements and approximations, the rate kernel becomes

$$(116) \quad \begin{aligned} K^{QC}(t'') &= -\frac{2}{\hbar\beta} \left(\frac{M}{2\pi\hbar} \right)^{3N} \Im \int dQ_1 d\dot{Q}_1 \sum_{\gamma, \mu, \nu} \sum_{Q_t} \\ &\times \int_{\epsilon} d(\Delta Q) \exp \left[-iM\dot{Q}_1 \cdot \Delta Q / \hbar \right] \rho_{\mu_2\nu}(Q_1 + \Delta Q, Q_1) \\ &\times T_{\gamma}^* [Q_t] T_{\mu} [Q_t] \chi_{\gamma_2\mu_1}(Q_{t''}) \chi_{\nu\gamma_1}(Q_1) . \end{aligned}$$

Using the Jacobian in Eq. (115), we have transformed the integral over Q_3 in Eq. (112) into an integral over \dot{Q}_1 , thereby eliminating the ‘‘root’’ search. The path Q_t is got by solving Pechukas equations with either γ or μ states. The sum over Q_t arises because the solution to this Pechukas equation subject to (Q_1, \dot{Q}_1) is nonunique. The high temperature approximation to the canonical density matrix $\rho_{\mu_2\nu}$ is

$$(117) \quad \left(\frac{M}{2\pi\hbar\beta} \right)^{\frac{3N}{2}} \exp \left[-\frac{M}{2\hbar^2\beta} (\Delta Q)^2 \right] \exp [-\beta E_{\mu_2}(Q_1)] \delta_{\mu_2\nu}$$

If the temperature is high enough that $R_{\epsilon} > (2\hbar^2\beta/M)^{1/2}$, then we can replace $\int_{\epsilon} d(\Delta Q)$ within Eq. (116) by $\int d(\Delta Q)$, an integral over all ΔQ . Evaluating this integral, we obtain the mixed quantum-classical rate kernel

$$(118) \quad \begin{aligned} K^{QC}(t'') &= -\frac{2}{\hbar\beta} \left(\frac{M}{2\pi\hbar} \right)^{3N} \Im \int dQ_1 d\dot{Q}_1 \sum_{\gamma\mu} \rho^{\mu_2}(Q_1, \dot{Q}_1) \\ &\times T_{\gamma}^* [Q_t] T_{\mu} [Q_t] \chi_{\gamma_2\mu_1}(Q_{t''}) \chi_{\mu_2\gamma_1}(Q_1) , \end{aligned}$$

where

$$(119) \quad \rho^{\mu}(Q_1, \dot{Q}_1) = \frac{e^{[-\beta(M\dot{Q}_1^2/2 + E_{\mu}(Q_1))]} }{\sum_{\mu} \int dQ_1 d\dot{Q}_1 e^{[-\beta(M\dot{Q}_1^2/2 + E_{\mu}(Q_1))]} } .$$

Note that in this high temperature limit all coherence in the initial density matrix is lost.

While the zero back reaction approximation is generally not valid, within the context of the Pechukas equation, it is needed in order to reduce the rate kernel to a more tractable form. In Ref. [35] a variant of the Pechukas stationary phase analysis is presented which overcomes the problems described above without resorting to this approximation.

5.1. Nonadiabatic proton transfer. – The above discussion provided some insight into the approximations needed to reduce the rate kernel expression to a quantum-classical form. However, in order to obtain a computationally tractable scheme, further approximations are needed. We shall not discuss the reduction of Eq. (118) to an average over surface-hopping trajectories. Instead, we simply use Tully’s surface hopping method [28] to investigate nonadiabatic contributions to the proton transfer rate and mechanism. In this method an ensemble of trajectories is considered. For each member of the ensemble the time-dependent Schrödinger equation

$$(120) \quad i\hbar \frac{d|\Psi; R(t), t\rangle}{dt} = \hat{h}(R(t))|\Psi; R(t), t\rangle,$$

is solved by expanding in the instantaneous adiabatic eigenstates,

$$(121) \quad |\Psi; R(t), t\rangle = \sum_{\alpha} c_{\alpha}(t)|\alpha; R(t), t\rangle,$$

yielding the evolution equation for the coefficients

$$(122) \quad i\hbar \frac{dC_{\alpha}(t)}{dt} = (E_{\alpha} - E_0)C_{\alpha}(t) - i\hbar \sum_{\alpha'} \frac{P}{M} \cdot d_{\alpha\alpha'} C_{\alpha'}(t),$$

where $d_{\alpha\alpha'}$ and E_{α} have been defined previously and

$$(123) \quad C_{\alpha}(t) = c_{\alpha}(t) \exp\left(i \int_0^t dt' E_0(R(t'))/\hbar\right).$$

The classical degrees of freedom evolve by Newton’s equation of motion subject to Hellmann-Feynman forces during each molecular dynamics time step Δ that depend on instantaneous adiabatic eigenstates. In this algorithm the probability of a hop from state α to α' is given by

$$(124) \quad w_{\alpha\alpha'} = \gamma_{\alpha\alpha'} \theta(\gamma_{\alpha\alpha'}),$$

where

$$(125) \quad \gamma_{\alpha\alpha'} = \frac{-2\Re(\rho_{\alpha'\alpha}^*(t + \Delta)(P/M) \cdot d_{\alpha\alpha'}\Delta)}{\rho_{\alpha\alpha}(t + \Delta)}.$$

This algorithm was implemented to study the cluster proton transfer reaction and the details of the simulation method can be found in Ref. [25]. However, in the results presented here the adiabatic wave functions were expanded in a set of 99 hat functions instead of the Gaussian basis used in our earlier studies [25].

The analysis of the nonadiabatic dynamics data employed six trajectories of duration 3 ns. The solvent polarization $\Delta E(R)$, shown in Fig. 13 as a function of time in the course of a nonadiabatic reactive trajectory, signals transitions between the reactant and product states. The expectation value of the position of the proton $\bar{z}_p^n(t) = \langle n; R(t), t | q | n; R(t), t \rangle$ (Fig. 13 b) shows similar transitions. However, in the upper panel of this

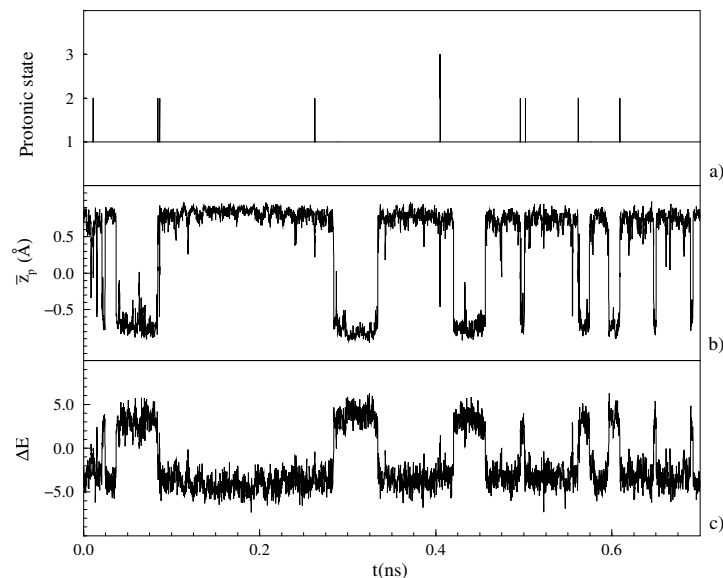


Fig. 13. – (a) Protonic state, (b) expectation value of the position of the proton \bar{z}_p and (c) solvent polarization (in units of $10^{-21}C/\text{\AA}$) as a function of time for a 67-molecule cluster.

figure we show the protonic state determined by the stochastic algorithm used to compute the Hellmann-Feynman forces for the classical particles. We observe that nonadiabatic transitions frequently occur when there is passage from reactant to product states or vice versa: there is significant breakdown of the adiabatic model. Such breakdown might be anticipated since the transition state configurations correspond to more nearly symmetrical solvation of the proton ion complex and one expects that the separation between the lowest adiabatic states will be smallest in this region. The three lowest adiabatic energies for a short time interval close to the transition state regime are shown in Fig. 14. The black dots denote the path of the proton in the proton state space. The three lowest eigenvalues show similar time variations. Proton hops between the different states occur by jump transitions when the difference between the energy states is close to 1-2 kT. In this regime there is strong mixing of the $C_\alpha(t)$ coefficients. The nonadiabatic transitions have consequences for the mechanism and rate of the reaction. In Fig. 15 the densities of the wavefunctions for the three lowest eigenstates are plotted at a point in time where the proton hops from state 1 to state 2. When the proton is found in an excited state, the proton density is more diffuse and as a result the Hellmann-Feynman forces lead to more symmetric solvent configurations which favour the transition state. Since the system tends to be found in the vicinity of the transition state when the proton is in an excited state, the number of hops and the proton recrossing attempts increase which alter the adiabatic dynamics transition state estimate of the rate and the transmission coefficient. The rate constant for the reaction was computed directly by counting the number of proton transfers in the nonadiabatic dynamics trajectories and is estimated to be $\kappa = 0.011\text{ps}^{-1}$. The dynamics for this model is dominated by the ground state. Since the adiabatic dynamics holds for the 90 percent of the time the changes in the rate due to surface hopping are not expected to be significant. Nonadiabatic dynamics can lead to a competition of effects: when the proton is found in an excited state the transition

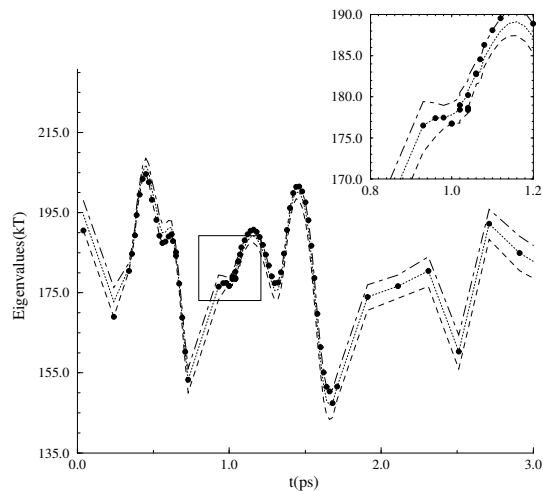


Fig. 14. – Instantaneous protonic adiabatic eigenstates as a function of time.

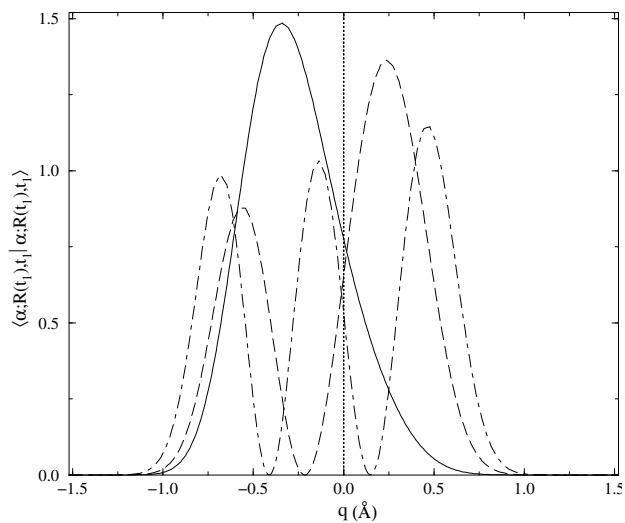


Fig. 15. – Instantaneous density of the adiabatic eigenfunctions. The ground and first and second excited states are represented by solid, dashed and dotted-dashed lines respectively.

state theory estimate of the rate is larger than when it is in the ground state; however, there is an increased number of recrossings of the transition state leading to a reduction of the transmission coefficient.

6. – Conclusions

Our ability to compute rate constants for activated processes remains at an early stage of development in spite of considerable recent progress in this area. For classical (and quantum) systems the formulation relies on the choice of species variables. While

the formal properties that such variables must satisfy are known, their forms are neither unique nor easy to specify in complex systems. When deviations from transition state theory are large the break-up of the rate constant expression into a transition state theory part and a transmission coefficient may not lead to an efficient computational algorithm.

For classical mechanical systems in the linear response regime, the dynamics and the rate formalism are well defined. The mixed quantum-classical regime, which provides the most promise for simulations of condensed phase rate processes with quantum character, has the least well-developed formalism. Not only do subtle questions about the nature of the dynamics remain, but efficient algorithms for simulating rare activated process need to be developed. The theory of rate processes will continue to be a challenging topic for some time.

* * *

This work was supported in part by a grant from the Natural Sciences and Engineering Research Council of Canada.

REFERENCES

- [1] S. R. de Groot and P. Mazur, *Non-Equilibrium Thermodynamics* (North-Holland, Amsterdam), 1962.
- [2] M. Emptage and J. Ross, *J. Chem. Phys.* **51** (1969) 252.
- [3] S. Golden, *Quantum Statistical Foundations of Chemical Kinetics*, (Oxford University Press, London), 1969.
- [4] R. Kubo, *J. Phys. Soc. Japan* **9** (1957) 570.
- [5] R. Kapral, *J. Chem. Phys.* **56** (1972) 1842; F. Garisto and R. Kapral, *J. Chem. Phys.* **58** (1973) 3129.
- [6] H. Mori, *Prog. Theor. Phys.* **33** (1965) 423.
- [7] R. Zwanzig, *Phys. Rev.* **124** (1961) 983.
- [8] R. Kapral, *Adv. Chem. Phys.* **48** (1981) 71.
- [9] M. Schell and R. Kapral, *J. Chem. Phys.* **75** (1981) 915.
- [10] J. Costley and P. Pechukas, *Chem. Phys. Lett.* **83** (1981) 139.
- [11] R. Kapral, S. Hudson and J. Ross, *J. Chem. Phys.* **53** (1970) 4387.
- [12] T. Yamamoto, *J. Chem. Phys.* **33** (1960) 281.
- [13] D. Chandler, *J. Chem. Phys.* **68** (1978) 2959.
- [14] E. Carter, G. Ciccotti, J. T. Hynes and R. Kapral, *Chem. Phys. Lett.* **156** (1989) 472.
- [15] G. M. Torrie and J. P. Valleau, *J. Comp. Phys.* **23** (1977) 187.
- [16] G. Ciccotti, M. Ferrario, D. Laria and R. Kapral, *Simulation of Classical and Quantum Activated Processes in the Condensed Phase*, in *Progress of Computational Physics of Matter: Methods, Software and Applications* edited by L. Reatto and F. Manghi, (World Scientific, New Jersey,) 1995, 150.
- [17] X.-G. Wu and R. Kapral, *J. Chem. Phys.* **91** (1989) 5528.
- [18] H. Kramers, *Physica*, **7** (1940) 284.
- [19] I. L'Heureux and R. Kapral, *J. Chem. Phys.* **88**(1988) 7468; *ibid.* **90** (1989) 2453; J. M. Porrà, J. Masoliver, K. Lindenberg, I. L'Heureux and R. Kapral, *Phys. Rev. A* **45** (1992) 6092; X.-G. Wu, I. L'Heureux and R. Kapral, *Chem. Phys. Lett.* **176** (1991) 242.
- [20] S. Consta and R. Kapral, unpublished.
- [21] J. Straub and B.J. Berne, *J. Chem. Phys.* **83** (1985) 1138.
- [22] M. J. Ruiz-Montero, D. Frenkel and J. J. Brey, *Mol. Phys.* **90** (1997) 925.
- [23] E. Wigner, *Phys. Rev.* **40** (1932) 749.
- [24] K. Imre, E. Özizmir, M. Rosenbaum and P. F. Zwiefel, *J. Math. Phys.* **5** (1967) 1097.

- [25] S. Consta and R. Kapral, *J. Chem. Phys.* **104** (1996) 4581; *ibid.* **101** (1994) 10908.
- [26] D. Laria, G. Ciccotti, M. Ferrario and R. Kapral, *J. Chem. Phys.* **97** (1992) 378; H. Azzouz and D. Borgis, *J. Chem. Phys.* **98** (1993) 7361; D. Borgis, G. Tarjus and H. Azzouz, *J. Phys. Chem.* **96** (1992) 3188; *J. Chem. Phys.* **97** (1992) 1390.
- [27] R. A. Marcus and N. Sutin, *Biochim. Biophys. Acta* **811** (1985) 265; A. Warshel, *J. Am. Chem. Soc.*, **86** (1982) 2218.
- [28] J. C. Tully, *J. Chem. Phys.* **93** (1990) 1061; J. C. Tully, *Int. J. Quantum Chem.* **25** (1991) 299; S. Hammes-Schiffer and J. C. Tully, *J. Chem. Phys.* **101** (1994) 4657.
- [29] L. Xiao and D. F. Coker, *J. Chem. Phys.* **100** (1994) 8646; D. F. Coker and L. Xiao, *J. Chem. Phys.* **102** (1995) 496; H. S. Mei and D.F. Coker, *J. Chem. Phys.* **104** (1996) 4755.
- [30] F. Webster, P. J. Rossky, and P. A. Friesner, *Comp. Phys. Comm.* **63** (1991) 494; F. Webster, E. T. Wang, P. J. Rossky, and P. A. Friesner, *J. Chem. Phys.* **100** (1994) 483.
- [31] E. R. Bittner and P. J. Rossky, *J. Chem. Phys.* **103** (1993) 8130 (1995).
- [32] P. Pechukas, *Phys. Rev.* **181** (1969) 166, 174.
- [33] W. H. Miller, *J. Chem. Phys.* **95** (1991) 9428.
- [34] E. J. Heller, *J. Chem. Phys.* **94** (1991) 2723, 9431.
- [35] J. L. McWhirter, *J. Chem. Phys.*, submitted.